GEOPHYSICS, VOL. 72, NO. 5 (SEPTEMBER-OCTOBER 2007); P. SM19–SM34, 12 FIGS.
10.1190/1.2757616

3D diffraction modeling of singly scattered acoustic wavefields based on the combination of surface integral propagators and transmission operators

Milana A. Ayzenberg[1], Arkady M. Aizenberg[2], Hans B. Helle[3], Kamill D. Klem-Musatov[2], Jan Pajchel[4], and Bjørn Ursin[1]

ABSTRACT

We present an improved method for modeling 3D acoustic wavefields scattered at smooth curved interfaces. The approach is based on a high-frequency approximation of surface integral propagators and a correct description of their boundary values in terms of transmission operators. The main improvement is a uniform local approximation of these operators in the form of effective reflection and transmission coefficients. We show that the effective coefficients represent a generalization of the plane-wave coefficients widely used in conventional seismic modeling, even for the case of curved reflectors, nonplanar wavefronts, and finite frequencies. The proposed method is capable of producing complex wave phenomenas, such as caustics, edge diffractions, and head waves. Seismograms modeled for even simple models reveal significant errors implicit in the plane-wave approximation. Comparison of modeling based on effective coefficients with the analytic solution reveals errors less than 4% in peak amplitude at seismic frequencies.

INTRODUCTION

Interest in 3D seismic modeling is increasing because of its applicability in forward and inverse problems (Ursin, 2004). In models with slowly varying geometry and properties, seismic wavefields can be computed using conventional methods. The situation is significantly different when the aim is to model the scattering in geologically complex areas. In this case, the Kirchhoff integral approach is one of the most powerful analytical methods (Ursin and Tygel, 1997; Schleicher et al., 2001). The approach is potentially capable of reproducing complex wave events, such as caustic triplications and diffracted waves.

The Kirchhoff integral approach implies knowledge of Green's function and two boundary values of the scattered wavefield and its directional derivative at the reflectors (Kleinman and Martin, 1988; Costabel and Stephan, 1990). In relatively simple media, the boundary values and the Green's function can be described by oscillatory functions using asymptotic ray theory (Červený, 2001), the perturbation method (Ursin and Tygel, 1997), and others. In these cases, asymptotic methods can be applied to the Kirchhoff integral (Frazer and Sen, 1985). In geologically complex media, standard Kirchhoff techniques encounter a serious pitfall, namely the boundary values and the Green's function can be evaluated only by expensive numerical techniques. Therefore it is necessary to seek methods of evaluating the surface integral propagators that avoid direct computation of the Green's function. Here, we utilize the tip wave superposition method (TWSM), which allows evaluating a high-frequency approximation of the propagators. The method was initially introduced for wave propagation in homogeneous media by Klem-Musatov and Aizenberg (1985); Klem-Musatov et al. (1993, 1994); and was later modified to a form invariant to medium heterogeneity by Aizenberg et al. (1996).

The boundary values are evaluated heuristically by multiplication of the incident wavefield and its directional derivative with the plane-wave reflection or transmission coefficient (Aki and Richards, 2002). This approach faces various problems because the assumption of planar incident waves is reasonable only for weak contrasts, small incidence angles, and relatively smooth reflectors. It is a well-known fact that the plane-wave coefficients do not account for complex wave phenomena such as near- and supercritical reflections/transmissions, but instead cause diffraction artifacts often clearly

Manuscript received by the Editor November 29, 2006; revised manuscript received March 23, 2007; published online August 23, 2007.
[1]Norwegian University of Science and Technology, Department of Petroleum Engineering and Applied Geophysics, Trondheim, Norway. E-mail: milana.ayzenberg@ipt.ntnu.no; bjorn.ursin@ntnu.no.
[2]Institute of Petroleum Geology and Geophysics SB RAS, Novosibirsk, Russia. E-mail: aizen@uiggm.nsc.ru; kamill@uiggm.nsc.ru.
[3]Odin Petroleum AS, High Technology Center in Bergen, Bergen, Norway. E-mail: hans.helle@odin-petroleum.no.
[4]Norsk Hydro AS, O&E Research Centre, Bergen, Norway. E-mail: jan.pajchel@hydro.com.

present in synthetic seismograms. This issue has been thoroughly discussed by Kampfmann (1988); Wenzel et al. (1990); and Sen and Frazer (1991).

The state of the art in the description of reflection/transmission phenomena is as follows. In homogeneous media separated by a plane interface, the reflected/transmitted wavefields can be decomposed into plane waves. This leads to the exact description of the reflection-transmission by a double convolution containing the plane-wave coefficients in the Fourier integral (e.g., Berkhout, 1987). To account for infinite interfaces of arbitrary geometry separating heterogeneous media, a necessary generalization of the plane-wave decomposition formula was introduced by Aizenberg and Ayzenberg (2002) and Aizenberg et al. (2005). By the generalized decomposition, the standard interface conditions can be rewritten as an equivalent system of reflection/transmission transforms (Klem-Musatov et al., 2004, 2005; Aizenberg et al., 2005). These transforms contain transmission operators in the form of convolutions over curved interfaces, which account for media heterogeneities, interface curvature, and frequency spectrum of the incident wavefield. In this paper, the transmission operators are reduced to the form of effective coefficients, which represent a generalization of the plane-wave coefficients and account for the proximity of the reflection/transmission point. Consequently, the effective coefficients correctly account for near- and supercritical effects, including the head waves, wavefront, and interface curvature, and response to the frequency spectrum of the incident wavefield (Aizenberg and Ayzenberg, 2002; Aizenberg et al., 2004, 2006a, b). We show that the plane-wave coefficients represent a degenerate case of the effective coefficients for precritical reflections and transmissions at weak-contrast interfaces.

Numerical tests show that, in spite of the complex description and yet time-consuming numerical implementation of the effective coefficients, the new theory has several useful applications. Obviously, it can be used for complex modeling tasks in heterogeneous layered media, and it provides improved understanding of complex wave phenomena. We believe the effective coefficients can be implemented successfully for solving inverse problems, such as AVO analysis and multiple removals.

In this paper, we propose an analytical approach to wave modeling based on the combination of propagators and transmission operators. We focus on relatively simple models to demonstrate the advantages of using the effective coefficients for Kirchhoff-type modeling, and the possibilities of the new approach. Comparison of synthetic seismograms illustrates the dramatic impact of using the improved reflection and transmission coefficients, even for relatively simple models. Elimination of artificial diffractions and the presence of head waves are the most significant effects seen in synthetic seismograms.

This paper is divided into three main parts. The first part contains theoretical results dealing with the singly scattered wavefield in terms of the sequential action of the propagators and transmission operators on the incident wavefield. The second part is devoted to approximations used in the propagators and transmission operators to obtain an algorithm for numerical modeling. The third part consists of the results of numerical modeling of singly scattered wavefields. All necessary theoretical calculations are provided in the appendices.

THEORY: SCATTERING AT A SINGLE INTERFACE

Statement of the transmission problem

We consider wave scattering at an infinite smooth curved interface S separating two homogeneous half-spaces D_1 and D_2 in $\mathbb{R}^3$. We use the vector notation $\mathbf{x}$ for spatial points in D_m ($m = 1,2$). The medium is described by the wave propagation velocities c_m and densities ρ_m. Assume all the curved parts of the interface lie inside a bounded volume, so that outside the volume, the interface is a horizontal plane.

Let a single point source be placed at an arbitrary point $\mathbf{x}^s$ that lies inside the half-space D_1. Then the time spectrum of the source wavefield $p_0(\mathbf{x},\omega)$ satisfies the acoustic wave equation

$$\nabla^2 p_0(\mathbf{x},\omega) + \frac{\omega^2}{c_1^2} p_0(\mathbf{x},\omega) = -\rho_1 \delta(\mathbf{x}^s,\mathbf{x}), \tag{1}$$

with the delta function $\delta(\mathbf{x}^s,\mathbf{x})$.

The stationary wavefields $p_m^{sc}(\mathbf{x},\omega)$ ($m = 1,2$) describe the time spectrum of the total scattered pressure field in D_m and satisfy the acoustic wave equation

$$\nabla^2 p_m^{sc}(\mathbf{x},\omega) + \frac{\omega^2}{c_m^2} p_m^{sc}(\mathbf{x},\omega) = 0. \tag{2}$$

At infinity, the wavefields satisfy the Sommerfeld radiation condition, which we do not specify. At the interface, the wavefields satisfy interface conditions which imply equality of the wavefields and normal accelerations at all points $\mathbf{x} \in S$ in the form

$$\begin{aligned} p_1^{sc}(\mathbf{x},\omega) + p_0(\mathbf{x},\omega) &= p_2^{sc}(\mathbf{x},\omega), \\ a_1^{sc}(\mathbf{x},\omega) + a_0(\mathbf{x},\omega) &= -a_2^{sc}(\mathbf{x},\omega), \end{aligned} \tag{3}$$

where $a_m^{sc}(\mathbf{x},\omega) = (1/\rho_m)\mathbf{n}_m \cdot \nabla p_m^{sc}(\mathbf{x},\omega)$ and $a_0(\mathbf{x},\omega) = (1/\rho_1)\mathbf{n}_1 \cdot \nabla p_0(\mathbf{x},\omega)$ are the normal accelerations, and $\mathbf{n}_m$ is the normal to the interface S directed toward D_m. To simplify the notations, we omit dependence on the angular frequency ω in this paper.

Single scattering in terms of propagators and transmission operators

In D_m, we define the fundamental solution (Green's function) $g_m(\mathbf{x},\mathbf{x}')$ as a solution of the equation

$$\nabla^2 g_m(\mathbf{x},\mathbf{x}') + \frac{\omega^2}{c_m^2} g_m(\mathbf{x},\mathbf{x}') = -\rho_m \delta(\mathbf{x},\mathbf{x}'), \tag{4}$$

satisfying a condition of total absorption. The condition of total absorption implies that the fundamental solution does not cause backward radiation after it has crossed the interface, i.e., it is absorbed by it. An implicit form of this condition is not known yet (see comments in Aizenberg and Ayzenberg, 2002 and Klem-Musatov et al., 2004). In our case, the fundamental solution is represented by a spherical wave having the explicit form

$$g_m(\mathbf{x},\mathbf{x}') = \rho_m \frac{e^{(i\omega/c_m)R(\mathbf{x},\mathbf{x}')}}{4\pi R(\mathbf{x},\mathbf{x}')}, \tag{5}$$

where $R(\mathbf{x},\mathbf{x}') = |\mathbf{x}' - \mathbf{x}|$ is the distance from point $\mathbf{x}$ to point $\mathbf{x}'$. According to equation 1, the source wavefield $p_0(\mathbf{x})$ coincides with the fundamental solution $g_1(\mathbf{x}^s,\mathbf{x})$.

Let $\mathbf{x}^r$ be an observation point. In Klem-Musatov et al. (2004) it is shown that the total scattered wavefield $p_m^{sc}(\mathbf{x}^r)$ can be rigorously represented as the sum

$$p_m^{sc}(\mathbf{x}^r) = p_m(\mathbf{x}^r) + \tilde{p}_m(\mathbf{x}^r), \tag{6}$$

where the term $p_m(\mathbf{x}^r)$ denotes the singly scattered wavefield and can be represented by the surface singular integral (Aizenberg et al., 2002; Aizenberg and Ayzenberg, 2002; Klem-Musatov et al., 2004)

$$p_m(\mathbf{x}^r) = \int\int_S \left[\frac{1}{\rho_m} \mathbf{n}_m(\mathbf{x}) \cdot \nabla\, g_m(\mathbf{x}^r, \mathbf{x}) b_{m(p)}(\mathbf{x}) - g_m(\mathbf{x}^r, \mathbf{x}) b_{m(a)}(\mathbf{x}) \right] dS(\mathbf{x}). \tag{7}$$

Physically, the two surface integrals in this formula denote the operators of the wave propagation through the medium. The total surface integral is often referred to as the Kirchhoff-type surface integral. The term $\tilde{p}_m(\mathbf{x}^r)$ denotes the sum of multiple scattered wavefields and can be represented by a surface singular integral similar to formula 7 with other boundary values (see corresponding details in Appendix A). In this paper, only the singly scattered wavefield $p_m(\mathbf{x}^r)$ is of interest to us.

We use the Chebyshev coordinates (x_1, x_2) covering the interface S (see details in Weatherborn, 1930 and do Carmo, 1976). The coordinate system generates a net on S with rhombic elements. The coordinates x_1 and x_2 coincide with the length along the curvilinear axes. The boundary values in formula 7 can be represented as the action of the operator

$$\left(\frac{\omega}{2\pi}\right)^2 \int\int_Q \int\int_S k_{mn}(q) e^{i\omega[(x_1 - x_1')q_1 + (x_2 - x_2')q_2]} \times dx_1' dx_2' dq_1 dq_2$$

on the boundary values of the source pressure $p_0(\mathbf{x}')$ and acceleration $a_0(\mathbf{x}')$ (Aizenberg et al., 2002, 2005; Klem-Musatov et al., 2004). The spatial spectra $k_{mn}(q)$ are similar to the classical plane-wave reflection (when $m = n$) and transmission (when $m \neq n$) coefficients (Aki and Richards, 2002):

$$k_{11}(q) = \frac{\frac{1}{\rho_1}\sqrt{\frac{1}{c_1^2} - q^2} - \frac{1}{\rho_2}\sqrt{\frac{1}{c_2^2} - q^2}}{\frac{1}{\rho_1}\sqrt{\frac{1}{c_1^2} - q^2} + \frac{1}{\rho_2}\sqrt{\frac{1}{c_2^2} - q^2}},$$

$$k_{12}(q) = 1 - k_{11}(q),$$

$$k_{21}(q) = 1 + k_{11}(q),$$

$$k_{22}(q) = - k_{11}(q), \tag{8}$$

where q is the slowness component tangent to the interface at point $\mathbf{x}$ (see details in Appendix A), and Q is the infinite plane of tangent components of the slowness vector. After interchanging the integrations, the boundary values in formula 7 can be represented in the convolution form as

$$b_{m(p)}(\mathbf{x}) = (k_{m1} * p_0)(\mathbf{x}) = \frac{\omega^2}{2\pi} \int\int_S k_{m1}(\xi) p_0(\mathbf{x}') dx_1' dx_2',$$

$$b_{m(a)}(\mathbf{x}) = - (k_{1m} * a_0)(\mathbf{x}) = - \frac{\omega^2}{2\pi} \int\int_S k_{1m}(\xi) a_0(\mathbf{x}') dx_1' dx_2', \tag{9}$$

where $\xi = \omega r$ and $r = \sqrt{(x_1 - x_1')^2 + (x_2 - x_2')^2}$. Derivation of the relations 9 in a simpler case of a curved interface between two homogeneous media in a form different from the one given by Klem-Musatov et al. (2004) is provided in Appendix A. Notice that, in the particular case of a plane interface, the convolution $b_{1(p)}(\mathbf{x})$ coincides with equation VII-13 presented by Berkhout (1987).

The kernels $k_{mn}(\xi)$ in equation 9 correspond to reflection (when $m = n$) and transmission (when $m \neq n$), and are introduced by the Fourier or Bessel transforms by Aizenberg et al. (2002, 2005). Here, we rewrite them as the double Fourier-type integrals over the slowness components (q_1, q_2):

$$k_{mn}(\xi) = \frac{1}{2\pi} \int\int_Q k_{mn}(q) e^{i\omega[(x_1 - x_1')q_1 + (x_2 - x_2')q_2]} dq_1 dq_2. \tag{10}$$

ALGORITHM: TIP WAVE SUPERPOSITION METHOD WITH EFFECTIVE COEFFICIENTS

Tip wave superposition method

To calculate high-frequency approximations of the propagators in formula 7 we use the formulas of the tip wave superposition method (TWSM) introduced by Klem-Musatov and Aizenberg (1985) and Klem-Musatov et al. (1993, 1994). For this purpose, it is sufficient to implement the two following mathematical operations to formula 7. First, we reduce the integration to a sum of contributions from small elements of the surface of integration. Then we find an approximation of the singular kernels in each integral contribution such that the contribution from a curved element can be substituted by a contribution from a plane element. Good accuracy of the approximation can be achieved by choosing the element size smaller than a quarter of a wavelength. Aizenberg (1982, 1993a, b) shows that the sum of the contributions from small plane elements reduces to the main computational formula of the TWSM, i.e., the sum of the tip waves diverging from vertices of the plane elements.

We first implement the reduction of the integral formula (7) to a sum of separate integrals from small elements of the integration surface. Using the Chebyshev coordinate system introduced earlier, the reflecting interface S can be split into rhombic elements whose edges are formed by the coordinate lines. Then the singly scattered wavefield has the form of the sum of the wavefields $\Delta p_{m[p]}(\mathbf{x}^r)$ coming from pth rhombic element,

$$p_m(\mathbf{x}^r) = \sum_p \Delta p_{m[p]}(\mathbf{x}^r), \tag{11}$$

$$\Delta p_{m[p]}(\mathbf{x}^r) = \int\int_{\Delta S_{[p]}} \left[\frac{1}{\rho_m} \mathbf{n}_m(\mathbf{x}) \cdot \nabla\, g_m(\mathbf{x}^r, \mathbf{x}) b_{m(p)}(\mathbf{x}) - g_m(\mathbf{x}^r, \mathbf{x}) b_{m(a)}(\mathbf{x}) \right] dS(\mathbf{x}). \tag{12}$$

We show in Appendix B that, if the element size is small enough, the integral equation (12) over the element can be approximated by the integral over a plane projection $\Delta\Pi_{[p]}$ of the original rhombic element,

$$\Delta p_{m[p]}(\mathbf{x}^r) \cong \Delta\bar{p}_{m[p]}(\mathbf{x}^r) = \int\int_{\Delta\Pi_{[p]}} \left[\frac{1}{\rho_m}\mathbf{n}_{m[p]} \cdot \nabla\, g_m(\mathbf{x}^r,\mathbf{x}) b_{m(p)}(\mathbf{x}) - g_m(\mathbf{x}^r,\mathbf{x}) b_{m(a)}(\mathbf{x}) \right] d\mathbf{x}. \quad (13)$$

Each contribution in equation 13 has the form (Klem-Musatov et al., 1994)

$$\Delta\bar{p}_{m[p]}(\mathbf{x}^r) = b_{m[p]}(\mathbf{x}_{[p]}) e^{[i(\omega/c_m)R(\mathbf{x}_{[p]},\mathbf{x}^r)\cos\,\gamma(\mathbf{x}_{[p]})]} \times \left\{ \delta_{[p]} + \sum_{q=1}^{4} \left[\delta_{[pq]} f_{m[pq]}(\mathbf{x}^r) + \sum_{r=1}^{2} f_{m[pqr]}(\mathbf{x}^r) \right] \right\}, \quad (14)$$

where $\mathbf{n}_{m[p]}$ is the normal to $\Delta\Pi_{[p]}$, $\delta_{[p]} = 1$ or 0 in the illuminated or shadow zone, $\delta_{[pq]} = 1$ or 0 in the secondary illuminated or shadow zone, $\gamma(\mathbf{x}_{[p]})$ is the reflection or transmission angle, and $f_{m[pq]}(\mathbf{x}^r)$ and $f_{m[pqr]}(\mathbf{x}^r)$ are attenuation functions of the edge and tip waves described by the Rubinowicz-type integral in the case of uniform asymptotics in the boundary layer, and by the Fresnel and generalized Fresnel integrals in the case of nonuniform asymptotics (Aizenberg, 1993b; Klem-Musatov, 1994).

If we exclude the elements corresponding to $\delta_p = 1$ and $\delta_{pq} = 1$, then representation 11 becomes

$$p_m(\mathbf{x}^r) \cong \sum_{p:\delta_p=\delta_{pq}=0} \Delta\bar{p}_{m[p]}(\mathbf{x}^r), \quad (15)$$

where

$$\Delta\bar{p}_{m[p]}(\mathbf{x}^r) = b_{m[p]} \times (\mathbf{x}_{[p]}) e^{[i(\omega/c_m)R(\mathbf{x}_{[p]},\mathbf{x}^r)\cos\,\gamma(\mathbf{x}_{[p]})]} \sum_{q=1}^{4}\sum_{r=1}^{2} f_{m[pqr]}. \quad (16)$$

It can be shown that in the far-zone approximation the contributions $\Delta\bar{p}_{m[p]}(\mathbf{x}^r)$ are

$$\Delta\bar{p}_{m[p]}(\mathbf{x}^r) \cong g_m(\mathbf{x}^r,\mathbf{x}_{[p]}) \left[\frac{1}{\rho_m}\mathbf{n}_{m[p]} \cdot \nabla\, R(\mathbf{x}_{[p]},\mathbf{x}^r) \times \left(i\frac{\omega}{c_m} - \frac{1}{R(\mathbf{x}_{[p]},\mathbf{x}^r)} \right) b_{m(p)}(\mathbf{x}_{[p]}) - b_{m(a)}(\mathbf{x}_{[p]}) \right] \Delta\Pi_{[p]}, \quad (17)$$

where $\mathbf{x}_{[p]}$ is the central point of the corresponding element with the area $\Delta\Pi_{[p]}$.

Formula 16 represents the scattered wavefield as the superposition of the tip waves and is the key formula of the TWSM (Klem-Musatov and Aizenberg, 1985; Klem-Musatov et al., 1994). It also naturally explains the name of the method.

The method is computationally inexpensive, but requires storing large matrices containing information about the tip waves. This fact can be considered as the drawback, as well as the advantage of the approach. Storing the matrices requires sufficient disk space. At the same time, minor changes of the model do not require reevaluation of all matrices, which becomes particularly valuable in multilayered models.

Effective reflection and transmission coefficients

The serious problem with Kirchhoff-type modeling is the representation of the boundary values of the wavefield at curved interfaces. It is common to represent the boundary values as a product of the incident wavefield and the plane-wave coefficient, or its approximations, which have irregularities at critical angles. However, such an approach causes artifacts in the form of edge waves diffracted at the contours of critical points on the interface (Kampfmann, 1988; Wenzel et al., 1990; Sen and Frazer, 1991). The approach appears to be an appropriate approximation for relatively small incident angles, small curvatures of reflectors, and weak contrasts in the model parameters. Therefore this approach is widely used for modeling of the precritical reflections. For near critical and supercritical reflections, the assumption breaks down because of the essential difference between the exact solution and the high-frequency approximation. To overcome this problem, an exact description of the boundary values in terms of integral reflection and transmission operators was introduced by Klem-Musatov et al. (2004, 2005). A high-frequency approximation of these operators in the form of effective coefficients is included in the acoustic version of the TWSM (Aizenberg and Ayzenberg, 2002; Aizenberg et al., 2004). This has important consequences for effective elimination of the diffraction artifacts at critical angles and correct modeling of the head waves.

The integral representation (formula 7) is widely used for modeling the spatial wavefields. It implies knowledge of the values of the pressure field and corresponding acceleration in a small vicinity of the interface. Although no proof has yet been given, it is common to use an empirical assumption that the value of the reflected or transmitted wavefield at the interface equals the value of the source wavefield multiplied by a reflection or transmission coefficient. In conventional seismic modeling, the incident wavefield at each particular point of the interface is approximated locally by a plane-wave tangent to the wavefront and having the same incident angle. Therefore it seems natural to use the plane-wave coefficients for local description of the reflection or transmission (Ursin, 2004). For easier interpretation of the relations in equation 9 in terms of reflection or transmission coefficients, we reduce them to the form of multiplication:

$$b_{m(p)}(\mathbf{x}) = \chi_{m1}(\mathbf{x}) p_0(\mathbf{x}), \quad b_{m(a)}(\mathbf{x}) = -\chi_{1m}(\mathbf{x}) a_0(\mathbf{x}). \quad (18)$$

In the following, we refer to the coefficients $\chi_{mn}(\mathbf{x})$ as the effective reflection and transmission coefficients. They are given by the formulas,

$$\chi_{m1}(\mathbf{x}) = \frac{\omega^2}{2\pi}\int\int_S k_{m1}(\xi)\bar{p}_0(\mathbf{x}';\mathbf{x})dx_1'dx_2',$$

$$\chi_{1m}(\mathbf{x}) = -\frac{\omega^2}{2\pi}\int\int_S k_{1m}(\xi)\bar{a}_0(\mathbf{x}';\mathbf{x})dx_1'dx_2', \quad (19)$$

where

$$\bar{p}_0(\mathbf{x}';\mathbf{x}) = \frac{p_0(\mathbf{x}')}{p_0(\mathbf{x})},$$

$$\bar{a}_0(\mathbf{x}';\mathbf{x}) = \frac{a_0(\mathbf{x}')}{a_0(\mathbf{x})}. \quad (20)$$

In Appendix C, we show that the effective coefficients (formula 19) can be approximated as

$$\chi_{m1}(\mathbf{x}) \cong \chi_{m1}(q_s(\mathbf{x}), \xi_F^*(\mathbf{x})) = \frac{\omega^2}{2\pi}\int\int_S k_{m1}(\xi)\bar{p}_0^*(\mathbf{x}';\mathbf{x})dx_1'dx_2',$$

$$\chi_{1m}(\mathbf{x}) \cong \chi_{1m}(q_s(\mathbf{x}), \xi_F^*(\mathbf{x})) = -\frac{\omega^2}{2\pi}\int\int_S k_{1m}(\xi)\bar{a}_0^*(\mathbf{x}';\mathbf{x})dx_1'dx_2'. \quad (21)$$

The effective coefficients functionally depend on the values of a normalized associated wavefield $\bar{p}_0^*(\mathbf{x})$ and $\bar{a}_0^*(\mathbf{x})$ at the interface. The associated wavefield is built on the information provided by the source wavefield and represents a dominant-frequency approximation of the kernels (equation 10). At each point $\mathbf{x}$, the associated wavefield is represented by a spherical wave having an incident angle $\gamma^*(\mathbf{x})$ and the distance between the source and point $\mathbf{x}$ equal to $R^*(\mathbf{x}^s,\mathbf{x})$, which depends on both the wavefront and interface curvatures (see calculations in Appendix C). The dependence of the associated parameters on the actual incident angle $\gamma(\mathbf{x})$ and the distance $R(\mathbf{x}^s,\mathbf{x})$ is

$$\gamma^*(\mathbf{x}) = \gamma(\mathbf{x}), \quad R^*(\mathbf{x}^s,\mathbf{x}) = R(\mathbf{x}^s,\mathbf{x}) \times \frac{\left[1 - \frac{1}{2}\sin^2\gamma(\mathbf{x})\right]}{\left[1 - \frac{1}{2}\sin^2\gamma(\mathbf{x})\right] - \cos\gamma(\mathbf{x})R(\mathbf{x}^s,\mathbf{x})H_S(\mathbf{x})}. \quad (22)$$

Note that the definition of $R^*(\mathbf{x}^s,\mathbf{x})$ includes both the radius of the wavefront curvature $R(\mathbf{x}^s,\mathbf{x})$ and the mean interface curvature $H_S(\mathbf{x})$. At a plane reflecting interface, when $H_S(\mathbf{x}) = 0$, the associated wavefield coincides with the actual incident wavefield. It is known that information about the wavefront and interface curvatures is absent in the plane-wave coefficients (see Appendix C). Therefore the effective coefficients generalize the plane-wave coefficients to the case of nonplane wavefront of the source wavefield, finite dominant frequency, and curved interface. However this generalization is not limited by elementary amplitude regularization and phase correction of reflected or transmitted wavefields in the near- or postcritical domains. In contrast to the propagators, the action of the transmission operators leads to the generation of new wavefields with different kinematics, in particular, head waves.

To illustrate the difference between the effective and plane-wave coefficients, we give examples for the case of plane interface at depth of 1 km between two homogeneous layers with velocity c_1 = 2 km/s and density ρ_1 = 2.0 g/cm^2 above the interface and velocity c_2 = 4 km/s and density ρ_2 = 2.0 g/cm^2 below the interface. The incident wave is generated by a point source placed at the point with the coordinates $\mathbf{x}^S = (0,0,0)$. The effective reflection coefficient as function of incident angle is shown in Figure 1. The four graphs are computed for frequencies of 0.32 Hz, 3.2 Hz, 32 Hz, and 320 kHz. The plane-wave reflection coefficient is shown for comparison. The critical incident angle is at 30°. The oscillations of the effective coefficient in the supercritical domain correspond to interference of the pure reflected wave and head wave. For higher frequencies, the effective coefficient approaches the plane-wave coefficient, but preserves the smooth behavior.

Computation of the effective coefficients is naturally more time-consuming than computation of the plane-wave coefficients. Therefore the choice of the appropriate coefficient is the tradeoff between computational speed and quality. We assume that the plane-wave coefficients give acceptable quality of the modeling results for weak-contrast interfaces and small offsets. Modeling of strong-contrast interfaces and large offsets limits the validity of the plane-wave coefficients and makes it necessary to use the effective coefficients. This issue is discussed in detail and illustrated in the next section devoted to the modeling results.

NUMERICAL SIMULATION

Here we present results of numerical simulation of the 3D scattered wavefields. The tests comprise synthetic modeling of the wavefields singly reflected and transmitted by smooth curved interfaces between two homogeneous half-spaces. In this section, we use the global Cartesian coordinates (x,y,z).

Simulations are carried out in the temporal frequency domain followed by a standard algorithm for the fast Fourier transform. In all the tests, we use the impulse form

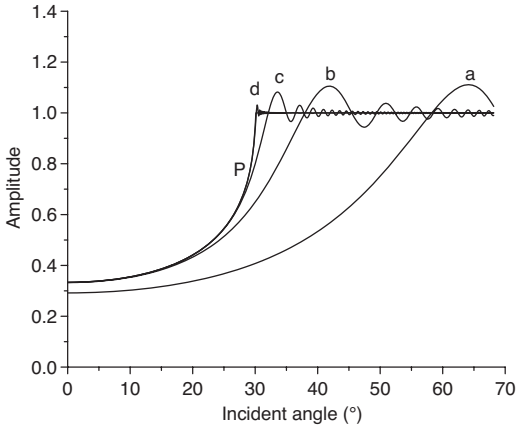

Figure 1. Modulus of the effective reflection coefficient versus incident angle for frequencies (a) 0.32 Hz, (b) 3.2 Hz, (c) 32 Hz, and (d) 320 kHz, in comparison to modulus of the plane-wave reflection coefficient (P).

$$F(t) = -\,e^{-p^2/\pi^2}\sin p, \quad p = 2\pi\frac{t - t_0}{T}, \tag{23}$$

where $t_0 = 0.064$ s is the time shift to the wavelet central point, and $T = 0.032$ s is the wave period. The wavelet shape and its spectrum are shown in Figure 2.

Modeling of single reflection

Three tests have been carried out to model the reflected wavefields.

Test model 1

The first test is carried out for the simplest model, which is a plane interface separating two homogeneous media. The purpose of this test is to estimate the accuracy of the high-frequency approximation of the Kirchhoff-type integral and the effective coefficient. The exact modeling is carried out using a Weyl-type integral representation (the phase-shift modeling).

We assume that the point source is situated at point $\mathbf{x}^s = (0,0,0)$. The receiver array is placed horizontally along the x-axis. The first receiver is at the source point and the last is at an offset of 2.5 km. The horizontal reflecting plane is situated at a depth $z = -1$ km. The upper half-space has a velocity $c_1 = 2$ km/s and density $\rho_1 = 2.0$ g/cm^3; the lower half-space has a velocity $c_2 = 4$ km/s and density $\rho_2 = 2.0$ g/cm^2. The model, source position, and data window are shown in Figure 3.

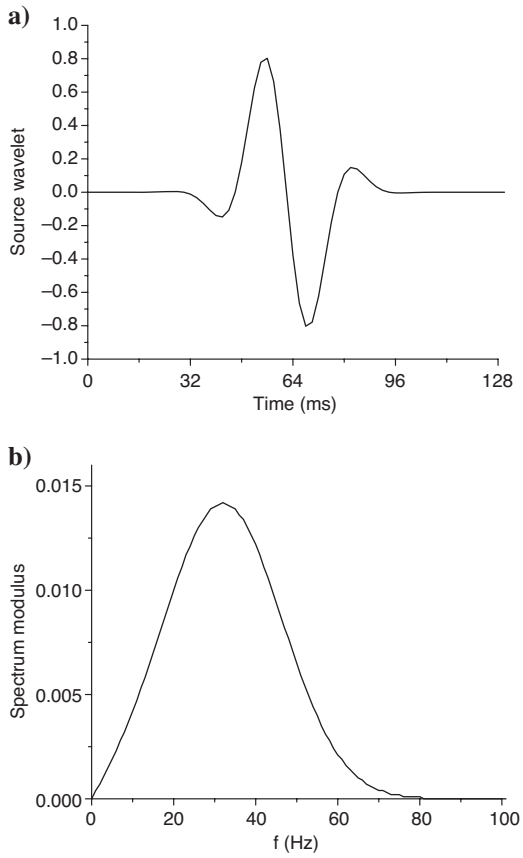

Figure 2. (a) Wavelet for 32-Hz dominant frequency and (b) its spectrum.

In Figure 4a and b, we show synthetic seismograms computed with the plane-wave and effective reflection coefficients, respectively. We see that the reflection in Figure 4a is seriously distorted by a strong diffraction event because of the discontinuity in the plane-wave reflection coefficient (see Figure 1) occurring at the critical reflection points confined to a circle of radius 0.57 km in the reflector plane.

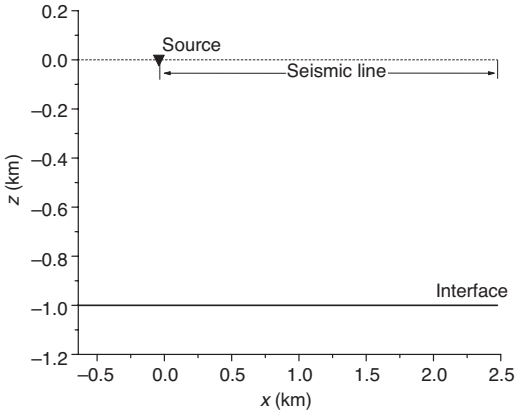

Figure 3. Model 1. Plane interface.

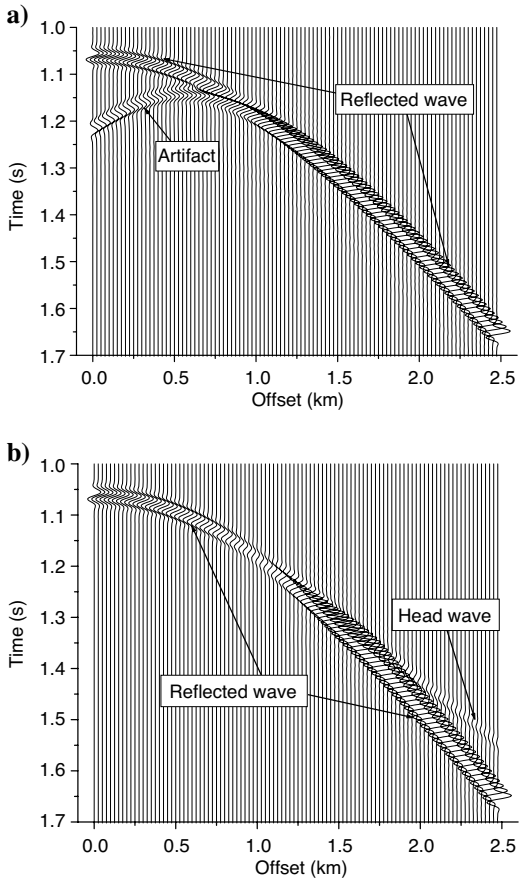

Figure 4. Model 1. Modeling with (a) plane-wave and (b) effective coefficients.

The amplitude of this artifact decreases with reduced velocity contrast across the interface, but is still present, as expected, because the integral interprets points of discontinuity of the boundary values as diffraction points, and therefore the diffraction event is implicit in the plane-wave approximation. By introducing the effective reflection coefficient, with continuous behavior, the diffraction artifact is eliminated and the head wave appears as shown in Figure 4b.

The latter clearly indicates that our modeling method using effective coefficients is qualitatively correct. To obtain a quantitative estimation of the correctness of reproduced reflected and head-wave amplitudes, we have chosen three traces corresponding to precritical, near-critical, and postcritical offsets. Trace comparison is shown in Figure 5. We estimate the errors implied by the TWSM approximations to be less than 4%.

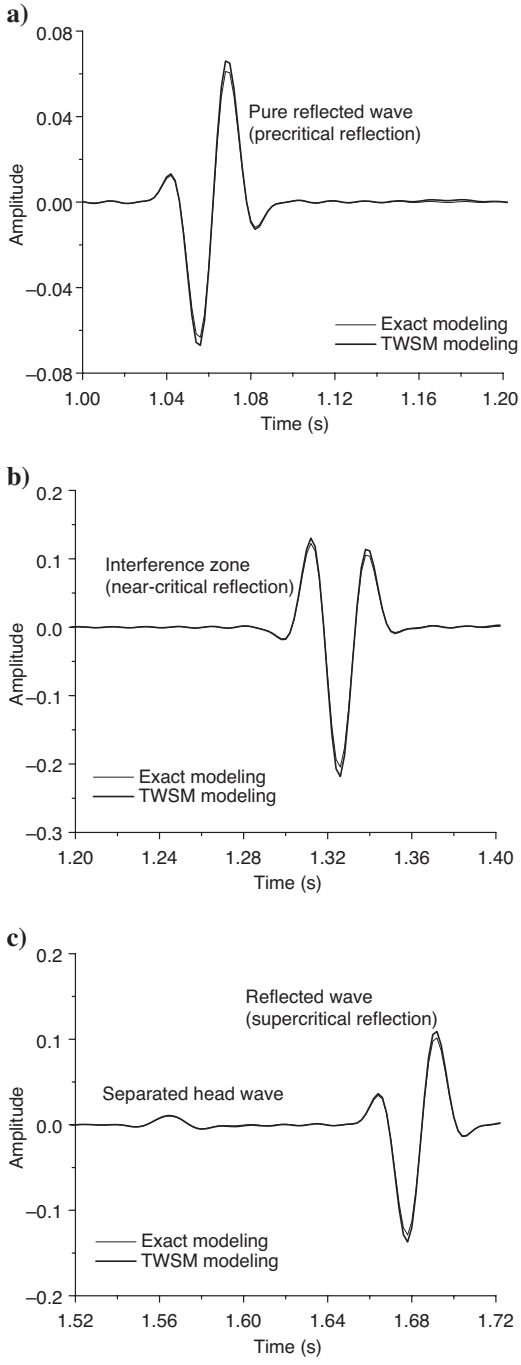

Figure 5. Model 1. Trace comparison for (a) pre-, (b) near-, and (c) postcritical offsets.

Test model 2

The second test is carried out with a smooth anticline interface separating the two half-spaces. The point source is placed at point $\mathbf{x}^s = (0,0,0)$. The receiver array is placed horizontally along the x-axis. The first receiver is at the source point and the last is at an offset of 2 km. The reflecting plane is described by the formula $z = -1 + 0.1e^{-16(x^2+y^2)}$ km. The upper half-space has a velocity $c_1 = 2$ km/s and density $\rho_1 = 2.0$ g/cm^3; the lower half-space has a velocity $c_2 = 4$ km/s and density $\rho_2 = 2.0$ g/cm^3. The model, source position, and data window are shown in Figure 6a. Figure 6b shows the cosine of the incident angle.

From the cosine of the incident angle in Figure 6b, we find a strip of supercritical incident angles formed between the two points with horizontal coordinates $x = 0.192$ km and $x = 0.288$ km. At the plane interface beyond the syncline parts, we find the same supercritical domain as in test 1. As demonstrated in Figure 7a, strong artificial diffraction events appear in this strip using the plane-wave reflection coefficient.

The seismogram computed with the effective reflection coefficient is given in Figure 7b. Along with the reflected wave, it contains

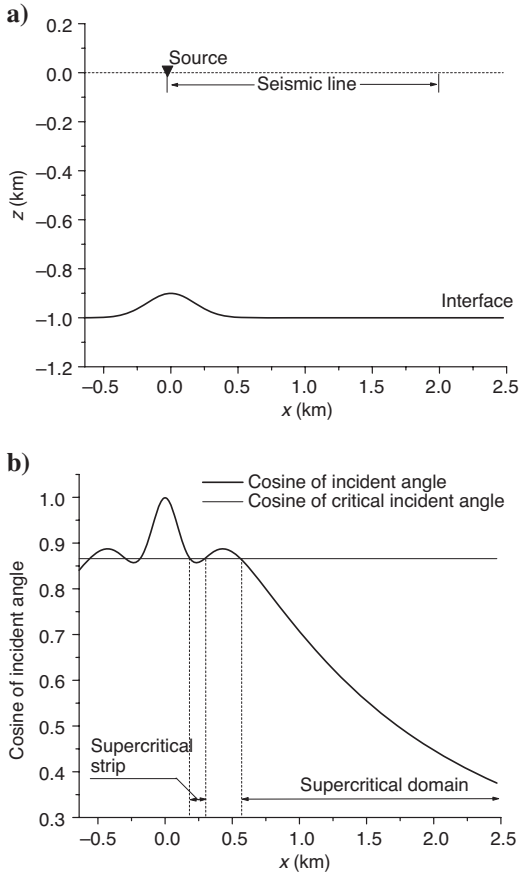

Figure 6. Model 2. (a) Gaussian bell anticline and (b) cosine of incident angle.

two head waves. The head wave generated in the supercritical domain where $x > 0.577$ km has the characteristic move-out for the head wave generated at the horizontal part of the boundary. The head wave generated in the supercritical strip between $x = 0.192$ km and $x = 0.288$ km has low apparent velocity with respect to the receiver array, and therefore arrives later than the reflected wave.

Test model 3

The third test is carried out also for a curved interface separating two half-spaces with the Gaussian anticline shifted with respect to the source position. The experiment in this test demonstrates in more detail the development of head waves and head-wave caustics at the slope of a Gaussian bell, as the slope and curvature change with the height of the bell.

The point source is placed at point $\mathbf{x}^s = (0,0,0)$. The receiver array is placed horizontally along the x-axis. The first receiver is at the source point and the last is at an offset of 4 km. The reflecting interface is described by the formula $z = -1 + \Delta z e^{-16[(x - 0.92)^2 + y^2]}$ km. The upper half-space has a velocity $c_1 = 2$ km/s and density $\rho_1 = 2.0$ g/cm^3; the lower half-space has a velocity $c_2 = 8$ km/s and density $\rho_2 = 2.0$ g/cm^3. The model, source position, and data window are shown in Figure 8a. Figure 8b shows the cosine of the incident angle.

The four seismograms in Figure 9 show the head-wave caustic formation with increasing height Δz of the Gaussian bell, for 0.005, 0.02, 0.04, and 0.08 km. A bright event develops in the pure reflected

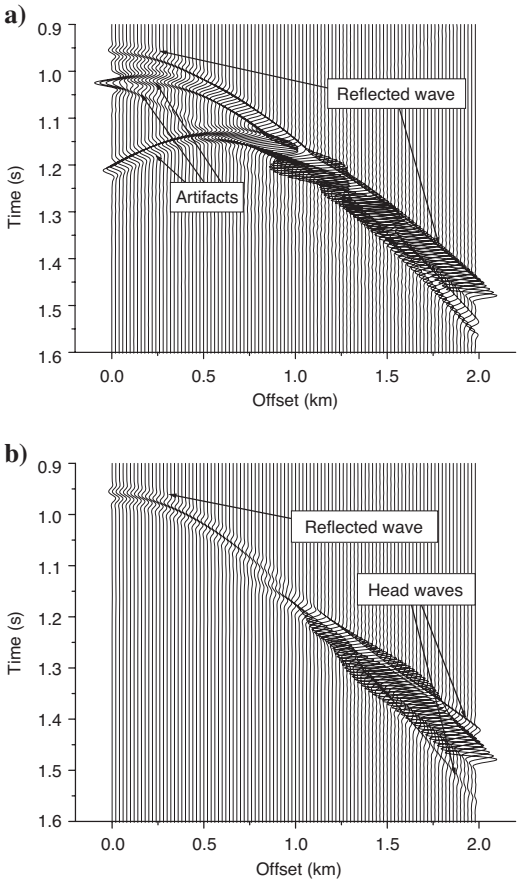

Figure 7. Model 2. Modeling with (a) plane-wave and (b) effective coefficients.

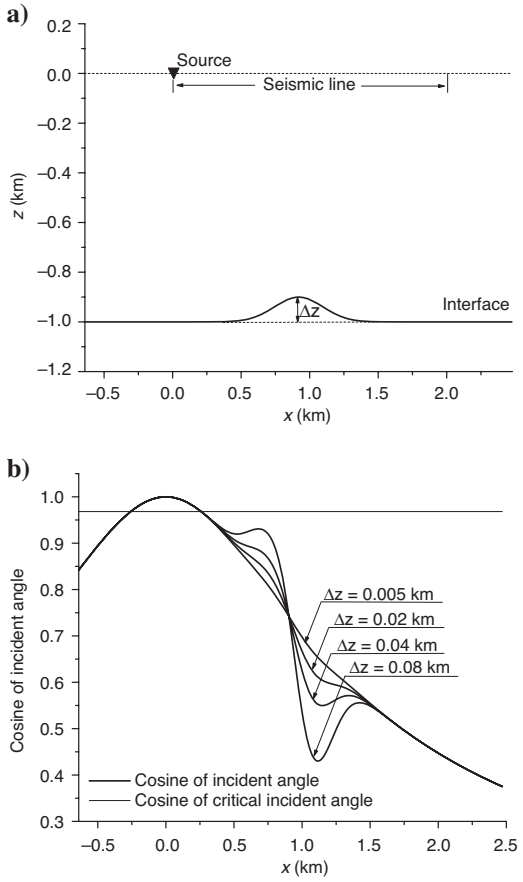

Figure 8. Model 3. (a) Gaussian bell with varying height Δz and (b) cosine of incident angle.

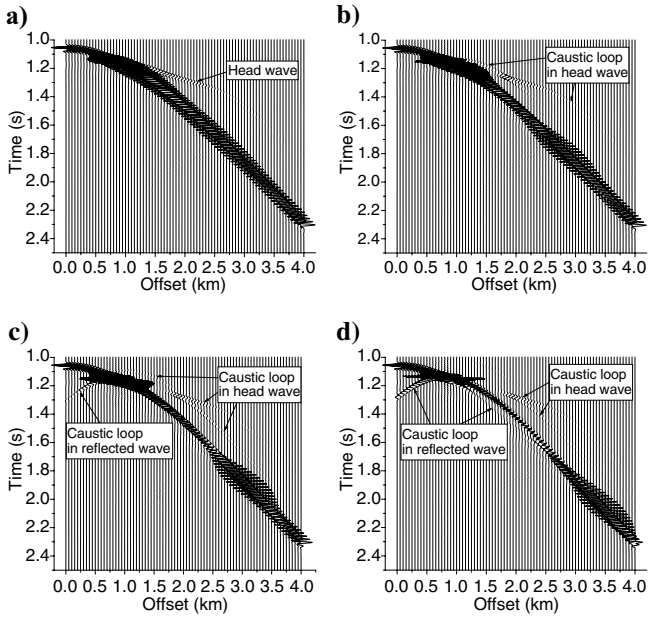

Figure 9. Model 3. Development of head-wave caustics for different values of Δz: (a) $\Delta z = 0.005$ km, (b) $\Delta z = 0.02$ km, (c) $\Delta z = 0.04$ km, and (d) $\Delta z = 0.08$ km.

arrival in the offset interval between $x = 0.5$ km and $x = 1.0$ km at traveltimes from 1.1 to 1.2 s for increasing Δz. For relatively large values of Δz, the formation of caustic triplication in both the pure reflected wave and the head wave is clearly seen.

Modeling of single transmission

Three tests are carried out to investigate the transmitted wavefields.

Test model 4

The point source is placed at point $\mathbf{x}^s = (0,0,0)$. The receiver array is placed horizontally along the x-axis. The first receiver is at the point with coordinates $(0,0,-2)$ km and the last is at an offset of 3 km. The medium model is chosen to be the same as in test 2. The model, source position, and data window are shown in Figure 10a. Figure 10b shows the modulus of the effective transmission coefficient (bold line) versus x for the dominant frequency of 32 Hz. The modulus of the plane-wave transmission coefficient (normal line) is given for comparison.

Seismograms modeled with the plane-wave and effective transmission coefficients are shown in Figure 11. The seismogram shown in Figure 11a is distorted by the artificial diffraction events caused by the curves of the critical transmission points with radii of 0.192, 0.288, and 0.577 km. Visual comparison of the two seismograms reveals a difference between the amplitudes of the transmitted waves. Modeling with the plane-wave transmission coefficient gives approximately 15% and 19% larger amplitude than that with the effective transmission coefficient at offsets of $x = 1.2$ km and $x = 2.4$ km, respectively.

Test model 5

The final tests are devoted to transmission at weak-contrast interfaces by reducing c_2 from 4.0 to 2.4 km/s. When using a model geometry exactly the same as in test 4, we find that the difference between the plane-wave and effective coefficient modeling exhibits negligibly small differences in the transmitted amplitudes and, therefore, are not shown. If the artificial diffractions are disregarded, we may conclude that transmission may be modeled equally well by the plane-wave coefficient in a weak-contrast environment with moderate interface curvature. However, to what extent is the effect of curvature significant in the case of weak contrast?

Test model 6

To answer this question, we change the interface shape from the one in test 5 to $z = -1 + 0.1e^{-64(x^2+y^2)}$ km, which increases the curvature by a factor of four at the interface vertically below the source. The resulting seismograms in Figure 12 reveal significant differences in response to the changes in interface geometry. The main differ-

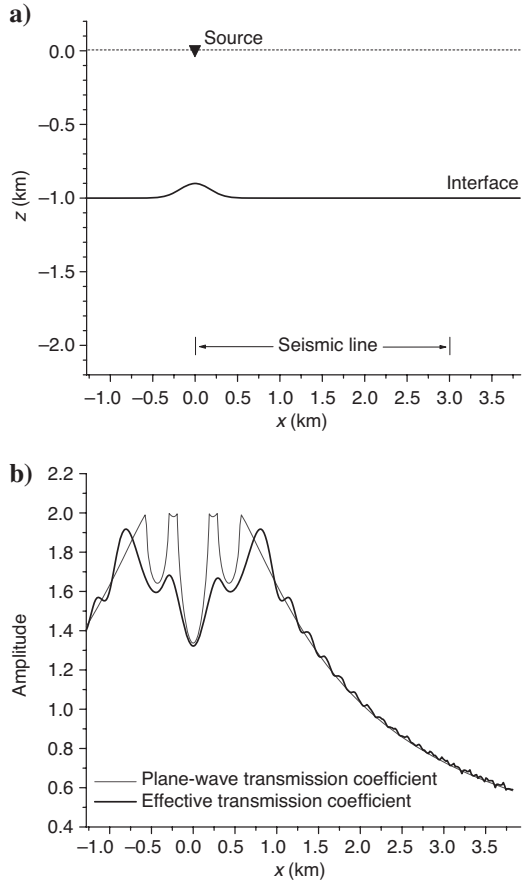

Figure 10. Model 4. (a) Gaussian bell anticline and (b) transmission coefficients in case of strong contrast and moderate curvature.

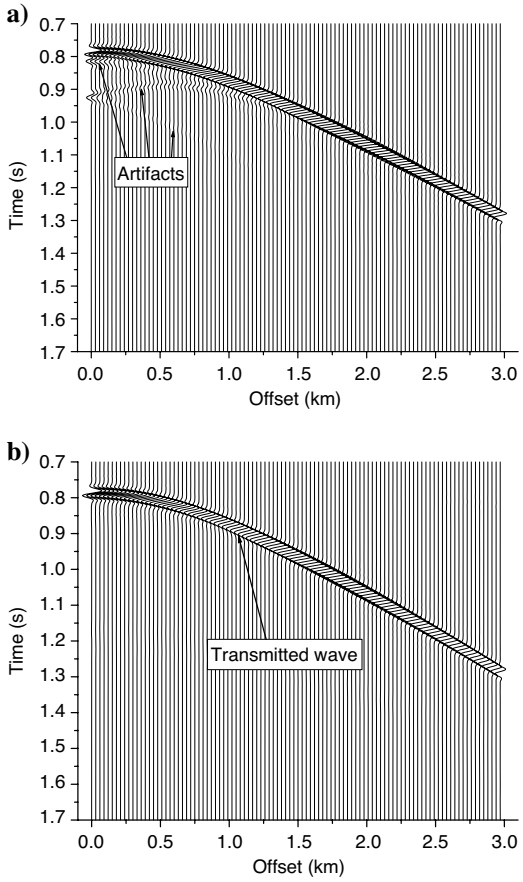

Figure 11. Model 4. Modeling with (a) plane-wave and (b) effective coefficients in case of strong contrast and moderate curvature.

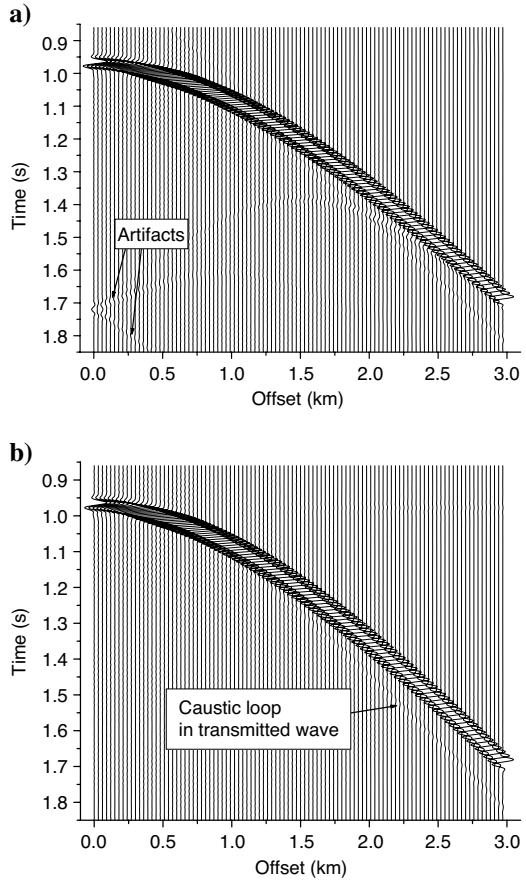

Figure 12. Model 6. (a) Modeling with plane-wave and (b) effective coefficients in case of weak contrast and significant curvature.

ences in the transmitted amplitudes are observed close to vertical incidence where the mean interface curvature is at its maximum. The amplitudes modeled with the plane-wave coefficient at the offsets close to zero are on average 8% larger than those modeled with the effective coefficients. For larger offsets, such as $x = 1.2$ km and $x = 2.4$ km, the difference in the amplitudes does not exceed 2%.

Notice that the weak event appearing at slightly later arrivals than the transmission is a caustic loop formed at the slope of the Gaussian cape.

CONCLUSIONS

We have presented an improved method for 3D seismic modeling in terms of surface integral propagators and transmission operators. The main improvement consists of the correct description of the boundary values of the propagators through the effective reflection and transmission coefficients. We have proven that, in the high-frequency approximation, the effective coefficients generalize the plane-wave coefficients. By numerical modeling, we have shown that the effective coefficients reproduce the complex wave events appearing at the near- and postcritical incident angles.

ACKNOWLEDGMENTS

The authors acknowledge the Russian Foundation for Basic Research (grant 03-05-64941), the Federal Agency of Science and Innovations (contract 02.445.11.7416), the Russian Science Program (grant RI-112/001/252), and Norsk Hydro a.s. (Bergen, Norway) for support of this study. We thank Brian Farrelly and anonymous reviewers for valuable comments.

APPENDIX A

TRANSMISSION OPERATORS AT A CURVED INTERFACE BETWEEN TWO HOMOGENEOUS ACOUSTIC MEDIA

Here we present a schematic explanation of the theoretical justification of the reflection and transmission relations 9. A rigorous theory for the scalar case is given by Klem-Musatov et al. (2004). Aizenberg et al. (2005) give a theory for acoustic inhomogeneous media.

It is well known (Felsen and Marcuvitz, 1973) that, in a homogeneous acoustic half-space D_m bounded by a plane infinite interface S, the spectral presentation for the total pressure wavefield can be represented by the sum of the two Weyl-type spectral integrals:

$$w_m^{\pm}(\mathbf{x}) = \frac{\omega^2}{2\pi} \int \int_Q w_m^{\pm}(q_1,q_2) e^{i\omega\tau_m^{\pm}(\mathbf{x})} dq_1 dq_2, \quad \text{(A-1)}$$

where $w_m^{\pm}(q_1,q_2)$ is the spatial spectrum of the integral for $x_3 = 0$, and $\tau_m^{\pm}(\mathbf{x}) = x_1q_1 + x_2q_2 \pm x_3\sqrt{1/c_m^2 - q^2}$ is the eikonal. To apply integrals A-1 to the spectral decomposition of the interface conditions (equation 3), it is necessary to define Cartesian coordinates (x_1,x_2) along the interface and a Cartesian rectangular coordinate x_3 along the normal $\mathbf{n}_m$. Let $x_3 = 0$ on the interface.

Let us show that the two integrals A-1 satisfy the acoustic wave equation 2. Direct substitution of the integrals into equation 2 shows that the integrand is equal to zero:

$$-\omega\left[\frac{1}{c_m^2} - (\nabla\tau_m^{\pm}(\mathbf{x}))^2\right] + i\nabla^2\tau_m^{\pm}(\mathbf{x}) = 0. \quad \text{(A-2)}$$

Because the identity holds true for any frequency ω, it is possible to represent this identity as the system of two independent relationships:

$$\frac{1}{c_m^2} - \frac{1}{c_m^2}(\nabla x_3)^2 - q_1^2(\nabla x_1)^2 - 2q_1q_2\,\nabla x_1 \cdot \nabla x_2 - q_2^2(\nabla x_2)^2 + q^2(\nabla x_3)^2 = 0,$$

$$q_1\nabla^2 x_1 + q_2\nabla^2 x_2 \pm \sqrt{\frac{1}{c_m^2} - q^2}\,\nabla^2 x_3 = 0. \quad \text{(A-3)}$$

In a nonorthogonal Cartesian coordinate system there are the well-known relationships $(\nabla x_1)^2 = (\nabla x_2)^2 = 1/\sin^2\Omega$, $\nabla x_1 \cdot \nabla x_2 = \cos\Omega/\sin^2\Omega$, and $(\nabla x_3)^2 = 1$, with Ω being the net angle. Therefore from the first relation in formula A-3, we obtain the definition of the tangent slowness component as

$$q = \frac{1}{\sin\Omega}\sqrt{q_1^2 + 2\cos\Omega q_1q_2 + q_2^2}. \quad \text{(A-4)}$$

In an orthogonal Cartesian coordinate system, when $\Omega = \pi/2$, the tangent slowness takes the simpler form $q = \sqrt{q_1^2 + q_2^2}$. The second

equation in formula A-3 is automatically satisfied because of the trivial relationships $\nabla^2 x_1 = \nabla^2 x_2 = \nabla^2 x_3 = 0$.

As shown by Aizenberg et al. (2005) the integrals A-1 can satisfy equation 2 at any point $\mathbf{R}(x_1^0, x_2^0, x_3)$ of an inhomogeneous medium in a small vicinity of the chosen point $\mathbf{x}^0(x_1^0, x_2^0)$ at the curved interface. We show this fact for the curved interface in a homogeneous medium schematically.

The actual curved interface S can be considered as a smooth continuous perturbation of a bounded part of a plane interface. As a result, the Cartesian coordinates (x_1, x_2) are deformed and transformed to the Chebyshev coordinates (x_1, x_2) (Weatherborn, 1930; do Carmo, 1976). Orientation of the normal $\mathbf{n}_m(\mathbf{x})$ and the net angle $\Omega(\mathbf{x})$ will now vary along the interface. The radius-vector of any point in the half-space can be described by the generalized formula

$$\mathbf{R}(x_1, x_2, x_3) = \mathbf{x}(x_1, x_2) + x_3 \mathbf{n}_m(\mathbf{x}), \tag{A-5}$$

where the undefined rectangular coordinate x_3 is directed along the normal $\mathbf{n}_m(\mathbf{x})$. The representation A-5 can be considered as a transformation from the Cartesian to curvilinear coordinates (x_1, x_2, x_3). This transformation is valid inside a very thin layer close to the interface because of the intersection of the normal axes.

At any chosen point $\mathbf{x}^0(x_1^0, x_2^0)$ of the Chebyshev coordinates, the relations $(\nabla x_1)^2 = (\nabla x_2)^2 = 1/\sin^2 \Omega(\mathbf{x}^0)$ and $\nabla x_1 \cdot \nabla x_2 = \cos \Omega(\mathbf{x}^0) / \sin^2 \Omega(\mathbf{x}^0)$ are valid. Because at this point $\nabla x_3 = \mathbf{n}_m(\mathbf{x})$, we see that $(\nabla x_3)^2 = 1$. Therefore, from the first equation in formula A-3 we obtain a value of the tangent component $q(\mathbf{x}^0)$ of the slowness, which is similar to equation A-4 and depends on the local net angle $\Omega(\mathbf{x}^0)$.

Because the values $\nabla^2 x_1$ and $\nabla^2 x_2$ cannot be equal to zero in the curvilinear coordinates (formula A-5), the second pair of equalities from formula A-3 should be considered as the equations with respect to some desired parameters defining the variable x_3. To introduce these parameters, we can write

$$x_3 = l + \beta^{\pm} \frac{l^2}{2} + \cdots, \tag{A-6}$$

where $\beta^{\pm}$ are the desired parameters, l is the metric length along the straight axis x_3, and the ellipses stands for third-order omitted terms. Substituting the value of x_3 from equation A-6 in $\nabla^2 x_3$, we represent the second pair of equations from formula, A-3 in the form

$$\nabla^2 x_3 = [\nabla_S \cdot \mathbf{n}_m](\mathbf{x}^0) + \frac{\partial^2 x_3}{\partial l^2} = \mp \frac{[q_1 \nabla^2 x_1 + q_2 \nabla^2 x_2](\mathbf{x}^0)}{\sqrt{\dfrac{1}{c_m^2} - q^2}}. \tag{A-7}$$

There is a well-known formula, $[\nabla_S \cdot \mathbf{n}_m](\mathbf{x}^0) = 2H(\mathbf{x}^0)$, where $H(\mathbf{x}^0)$ is the mean curvature of the interface (Weatherborn, 1930; do Carmo, 1976). Then accounting for the second derivative of equation A-6, one obtains from the identities A-7 the desired parameters,

$$\beta^{\pm} = 2H(\mathbf{x}^0) \mp \frac{[q_1 \nabla^2 x_1 + q_2 \nabla^2 x_2](\mathbf{x}^0)}{\sqrt{\dfrac{1}{c_m^2} - q^2}}. \tag{A-8}$$

It is clearly seen from equation A-8 that the variable scale along the axis x_3 is a necessary condition for the Weyl-type integrals to be solutions of the acoustic wave equation 2 in a small homogeneous vicinity of the curved interface.

It is shown by Aizenberg et al. (2005) that, at the interface, the following relations hold true:

$$\begin{aligned} p_1^{sc}(\mathbf{x}) + p_0(\mathbf{x}) &= w_1^+(\mathbf{x}) + w_1^-(\mathbf{x}), \\ p_2^{sc}(\mathbf{x}) &= w_2^+(\mathbf{x}) + w_2^-(\mathbf{x}), \\ a_1^{sc}(\mathbf{x}) + a_0(\mathbf{x}) &= \frac{1}{\rho_1} \frac{\partial [w_1^+(\mathbf{x}) + w_1^-(\mathbf{x})]}{\partial x_3}, \\ a_2^{sc}(\mathbf{x}) &= \frac{1}{\rho_2} \frac{\partial [w_2^+(\mathbf{x}) + w_2^-(\mathbf{x})]}{\partial x_3}. \end{aligned} \tag{A-9}$$

Substitution of equation A-9 into the interface conditions (equation 3) gives

$$\begin{aligned} &w_1^+(q_1, q_2) + w_1^-(q_1, q_2) = w_2^+(q_1, q_2) + w_2^-(q_1, q_2), \\ &\frac{i\sqrt{c_1^{-2} - q^2}}{\rho_1} [w_1^+(q_1, q_2) - w_1^-(q_1, q_2)] = \\ &\quad - \frac{i\sqrt{c_2^{-2} - q^2}}{\rho_2} [w_2^+(q_1, q_2) - w_2^-(q_1, q_2)]. \end{aligned} \tag{A-10}$$

Solving this system for the unknowns $w_m^+(q_1, q_2)$ and $w_m^-(q_1, q_2)$ independently, we obtain the solution in the spectral form:

$$w_m^{\pm}(q_1, q_2) = k_{m1}(q) w_1^{\mp}(q_1, q_2) + k_{m2}(q) w_2^{\mp}(q_1, q_2), \tag{A-11}$$

with the reflection and transmission coefficients as in equation 8. Substituting equation A-11 into the Weyl-type integrals A-1 for $x_3 = 0$ and then substituting the result into the first pair of relations from equation A-9, we obtain the first interface condition in the form of the transmission transform:

$$\begin{aligned} p_1^{sc}(\mathbf{x}) &= (k_{11} * p_0)(\mathbf{x}) + [(k_{11} * p_1^{sc})(\mathbf{x}) + (k_{12} * p_2^{sc})(\mathbf{x})] \\ &\quad - p_0(\mathbf{x}), \\ p_2^{sc}(\mathbf{x}) &= (k_{21} * p_0)(\mathbf{x}) + [(k_{21} * p_1^{sc})(\mathbf{x}) + (k_{22} * p_2^{sc})(\mathbf{x})]. \end{aligned} \tag{A-12}$$

The system A-10 can, by analogy, be solved for the acceleration spectra $(i\sqrt{c_m^{-2} - q^2}/\rho_m) w_m^+(q_1, q_2)$ and $-(i\sqrt{c_m^{-2} - q^2}/\rho_m) w_m^-(q_1, q_2)$ independently. Then we obtain relations similar to equation A-11,

$$\begin{aligned} &\pm \frac{i\sqrt{c_m^{-2} - q^2}}{\rho_m} w_m^{\pm}(q_1, q_2) \\ &\quad = -k_{1m}(q) \left[\mp \frac{i\sqrt{c_1^{-2} - q^2}}{\rho_1} w_1^{\mp}(q_1, q_2) \right] \\ &\qquad -k_{2m}(q) \left[\mp \frac{i\sqrt{c_2^{-2} - q^2}}{\rho_2} w_2^{\mp}(q_1, q_2) \right], \end{aligned} \tag{A-13}$$

Substituting equation A-13 into the Weyl-type integrals A-1 for $x_3 = 0$ and then substituting the result into the second pair of relations from equation A-9, we obtain the second interface condition in the form of the transmission transform:

$$a_1^{sc}(\mathbf{x}) = -(k_{11} * a_0)(\mathbf{x}) - [(k_{11} * a_1^{sc})(\mathbf{x}) + (k_{21} * a_2^{sc})(\mathbf{x})] - a_0(\mathbf{x}),$$
$$a_2^{sc}(\mathbf{x}) = -(k_{12} * a_0)(\mathbf{x}) - [(k_{12} * a_1^{sc})(\mathbf{x}) + (k_{22} * a_2^{sc})(\mathbf{x})]. \quad \text{(A-14)}$$

The first terms in the relations A-12 and A-14 coincide with the relations 9 and represent singly reflected and transmitted wavefields. The second terms in the relations A-12 and A-14 represent multiply reflected and transmitted wavefields which generate the term $\widetilde{p}_m(\mathbf{x}^r)$ in equation 6 (see details in Klem-Musatov et al., 2004 and Aizenberg et al., 2005).

APPENDIX B

PROPAGATOR APPROXIMATION IN TWSM

We show that two propagators in the contribution (equation 12) from a small element of the interface can be approximated by the first term of a local Taylor representation using the size of this element as the small parameter. Consider the contribution (equation 12) from a curved rhombic element. Draw the tangent plane to this element through its central point $\mathbf{x}_{[p]}$ and project the element to the plane to obtain a plane rhombic element $\Delta\Pi_{[p]}$. Then points on $\Delta S_{[p]}$ have coordinates $\mathbf{x} = (\bar{\mathbf{x}}, z(\bar{\mathbf{x}}))$, where $\bar{\mathbf{x}} = (x_1, x_2)$ are their projections on $\Delta\Pi_{[p]}$, and $z(\bar{\mathbf{x}})$ is the distance between $\Delta S_{[p]}$ and $\Delta\Pi_{[p]}$ along the normal $\mathbf{n}_m(\mathbf{x}_{[p]})$ to $\Delta\Pi_{[p]}$.

Provide a local Taylor representation for the normal $\mathbf{n}_m(\mathbf{x})$, the function $g_m(\mathbf{x}^r, \mathbf{x})$ and its normal derivative in the surface Chebyshev coordinates in a vicinity of $\mathbf{x}_{[p]}$ as

$$\mathbf{n}_m(\mathbf{x}) = \mathbf{n}_m(\mathbf{x}_{[p]}) + \partial_j \mathbf{n}_m(\mathbf{x}_{[p]})(x_j - x_{[p]j}) + \frac{1}{2}\partial_i\partial_j \mathbf{n}_m(\mathbf{x}_{[p]})(x_i - x_{[p]i})(x_j - x_{[p]j}),$$
$$g_m(\mathbf{x}^r, \mathbf{x}) = g_m(\mathbf{x}^r, \bar{\mathbf{x}}) + \varepsilon_{m(a)}(\mathbf{x}^r, \mathbf{x}),$$
$$\mathbf{n}_m(\mathbf{x}) \cdot \nabla\, g_m(\mathbf{x}^r, \mathbf{x}) = \mathbf{n}_m(\mathbf{x}_{[p]}) \cdot \bar{\nabla} g_m(\mathbf{x}^r, \bar{\mathbf{x}}) + \varepsilon_{m(s)}(\mathbf{x}^r, \mathbf{x}), \quad \text{(B-1)}$$

where

$$\varepsilon_{m(a)}(\mathbf{x}^r, \mathbf{x}) = \frac{1}{2}[\partial_3 g_m(\mathbf{x}^r, \mathbf{x}_{[p]})\partial_i\partial_j z(\mathbf{x}_{[p]})](x_i - x_{[p]i}) \times (x_j - x_{[p]j}),$$
$$\varepsilon_{m(s)}(\mathbf{x}^r, \mathbf{x}) = \frac{1}{2}[\partial_3\partial_3 g_m(\mathbf{x}^r, \mathbf{x}_{[p]})\partial_i\partial_j z(\mathbf{x}_{[p]})](x_i - x_{[p]i}) \times (x_j - x_{[p]j}) + \partial_j \mathbf{n}_m(\mathbf{x}_{[p]}) \cdot \nabla\, g_m(\mathbf{x}^r, \mathbf{x}_{[p]}) \times (x_j - x_{[p]j}) + \frac{1}{2}\partial_i\partial_j \mathbf{n}_m(\mathbf{x}_{[p]}) \cdot \nabla\, g_m(\mathbf{x}^r, \mathbf{x}_{[p]}) \times (x_i - x_{[p]i})(x_j - x_{[p]j}). \quad \text{(B-2)}$$

Accounting for formulas B-1 and B-2, we obtain

$$\Delta p_{m[p]}(\mathbf{x}^r) = \int\int_{\Delta\Pi_{[p]}} \left[\frac{1}{\rho_m}\mathbf{n}_m(\mathbf{x}_{[p]}) \cdot \bar{\nabla} g_m(\mathbf{x}^r, \bar{\mathbf{x}}) b_{m(p)}(\mathbf{x}) - g_m(\mathbf{x}^r, \bar{\mathbf{x}}) b_{m(a)}(\mathbf{x})\right] dS(\mathbf{x}) + \int\int_{\Delta S_{[p]}} \times [\varepsilon_{m(s)}(\mathbf{x}^r, \mathbf{x}) b_{m(p)}(\mathbf{x}) - \varepsilon_{m(a)}(\mathbf{x}^r, \mathbf{x}) b_{m(a)} \times (\mathbf{x})] d\mathbf{x}. \quad \text{(B-3)}$$

Independent of the representation of the boundary values $b_{m(p)}(\mathbf{x})$ and $b_{m(a)}(\mathbf{x})$, the second integral in formula B-3 is a small quantity of the order of $(\omega/c_1 l)^2$, where l is the characteristic size of the element, compared to the first integral. Therefore, for $(\omega/c_1 l)^2 \ll 1$, we can approximate

$$\Delta p_{m[p]}(\mathbf{x}^r) \cong \int\int_{\Delta\Pi_{[p]}} \left[\frac{1}{\rho_m}\mathbf{n}_m(\mathbf{x}_{[p]}) \cdot \bar{\nabla} g_m(\mathbf{x}^r, \bar{\mathbf{x}}) b_{m(p)}(\mathbf{x}) - g_m(\mathbf{x}^r, \bar{\mathbf{x}}) b_{m(a)}(\mathbf{x})\right] dS(\mathbf{x}). \quad \text{(B-4)}$$

This means that, for small enough elements, we can approximate the surface integral over curved elements $\Delta S_{[p]}$ by the surface integral over plane elements $\Delta\Pi_{[p]}$.

APPENDIX C

FRESNEL-ZONE APPROXIMATION OF THE EFFECTIVE COEFFICIENTS

Here we will prove that the effective coefficients essentially depend on two parameters: the lateral slowness $q_s(\mathbf{x})$ and a normalized radius of the Fresnel zone $\xi_F(\mathbf{x})$. Below we give a detailed study only of the effective coefficients for the pressure wavefields which are represented by the first integral in formula 19. Because of the similarity in analysis of the effective coefficients for the pressure and acceleration wavefields, for the latter, we provide only the final approximations. Note that the analysis provided here is carried out in the Chebyshev coordinates which are orthogonal at point $\mathbf{x}$. Because the result is expressed in term of invariants with respect to the net angle of the coordinate system, it remains valid in any curvilinear Chebyshev coordinate system as well.

Substitution of equation 10 into the first integral in the representation (formula 19) gives

$$\chi_{m1}(\mathbf{x}) = \left(\frac{\omega}{2\pi}\right)^2 \int\int\int\int_{S\times Q} k_{m1}(q)\bar{p}_0(\mathbf{x}';\mathbf{x}) \times e^{i\omega[(x_1 - x_1')q_1 + (x_2 - x_2')q_2]} dq_1 dq_2 dx_1' dx_2' = \int\int\int\int_{S\times Q} m(\mathbf{x}', q) e^{i\omega\varphi(\mathbf{x}', q_1, q_2)} dq_1 dq_2 dx_1' dx_2', \quad \text{(C-1)}$$

where

$$m(\mathbf{x}',q) = \left(\frac{\omega}{2\pi}\right)^2 \frac{R(\mathbf{x}^s,\mathbf{x})}{R(\mathbf{x}^s,\mathbf{x}')} k_{m1}(q),$$

$$\varphi(\mathbf{x}',q_1,q_2) = \frac{R(\mathbf{x}^s,\mathbf{x}') - R(\mathbf{x}^s,\mathbf{x})}{c_1} + (x_1 - x_1')q_1 + (x_2 - x_2')q_2. \quad \text{(C-2)}$$

Assume ω is the large parameter. Then we can apply the stationary phase method to the last integral in equation C-1 (Bleistein and Handelsman, 1975). The stationary phase point $(\mathbf{x}_s', q_{s1}, q_{s2})$ is found from the equations

$$\left.\frac{\partial\varphi(\mathbf{x}',q_1,q_2)}{\partial x_j'}\right|_{\mathbf{x}'=\mathbf{x}_s',q_1=q_{s1},q_2=q_{s2}} = \frac{1}{c_1}\frac{\partial R(\mathbf{x}^s,\mathbf{x}_s')}{\partial x_j'} - q_{sj} = 0,$$

$$\left.\frac{\partial\varphi(\mathbf{x}',q_1,q_2)}{\partial q_j}\right|_{\mathbf{x}'=\mathbf{x}_s',q_1=q_{s1},q_2=q_{s2}} = x_j - x_{sj}' = 0, \quad \text{(C-3)}$$

which are satisfied simultaneously for $j = 1,2$. The equations give the definition of the only stationary point as

$$q_{sj}(\mathbf{x}) = \frac{1}{c_1}\frac{\partial R(\mathbf{x}^s,\mathbf{x})}{\partial x_j'}, \qquad x_{sj}' = x_j. \quad \text{(C-4)}$$

From the relations C-4, it follows that the stationary phase point is $(\mathbf{x}_s', q_{s1}, q_{s2}) = (\mathbf{x}, (1/c_1)\partial R(\mathbf{x}^s,\mathbf{x})/\partial x_1', (1/c_1)\partial R(\mathbf{x}^s,\mathbf{x})/\partial x_2')$. Applying the stationary phase method, the integral representation C-1 can be approximated as

$$\chi_{m1}(\mathbf{x}) \sim \left(\frac{2\pi}{\omega}\right)^2 \frac{1}{\sqrt{|\det \mathbf{H}(\mathbf{x},q_{s1},q_{s2})|}} m(\mathbf{x},q_s) \times e^{i\omega\varphi(\mathbf{x},q_{s1},q_{s2}) + i\pi/4 \operatorname{sgn}\mathbf{H}(\mathbf{x},q_{s1},q_{s2})}, \quad \text{(C-5)}$$

where $q_s(\mathbf{x}) = \sin\gamma(\mathbf{x})/c_1 = \sqrt{q_{s1}^2(\mathbf{x}) + q_{s2}^2(\mathbf{x})}$, $q_{s1}(\mathbf{x}) = q_s(\mathbf{x})\cos\psi$, $q_{s1}(\mathbf{x}) = q_s(\mathbf{x})\sin\psi$. The matrix signature $\operatorname{sgn}\mathbf{H}(\mathbf{x},q_{s1},q_{s2})$ is equal to the difference between the number of positive and negative eigenvalues. For simplicity, we direct the coordinate axes to satisfy the condition $\partial^2 R(\mathbf{x}^s,\mathbf{x})/\partial x_1'\partial x_2' = 0$; then we use matrix of the second derivatives of the phase function $\varphi(\mathbf{x}',q_1,q_2)$,

$$\mathbf{H}(\mathbf{x},q_{s1},q_{s2}) = \left[\frac{\partial^2\varphi(\mathbf{x},q_{s1},q_{s2})}{\partial x_i'\partial q_j}\right] = \begin{pmatrix} \frac{1}{c_1}\frac{\partial^2 R(\mathbf{x}^s,\mathbf{x})}{\partial x_1'^2} & 0 & -1 & 0 \\ 0 & \frac{1}{c_1}\frac{\partial^2 R(\mathbf{x}^s,\mathbf{x})}{\partial x_2'^2} & 0 & -1 \\ -1 & 0 & 0 & 0 \\ 0 & -1 & 0 & 0 \end{pmatrix}. \quad \text{(C-6)}$$

Following any standard technique, the eigenvalues of the matrix $\mathbf{H}(\mathbf{x},q_{s1},q_{s2})$ can be found as $\lambda_i^{\pm} = (1/2c_1)\partial^2 R(\mathbf{x}^s,\mathbf{x})/\partial x_i'^2 \pm \sqrt{1 + ((1/2c_1)\partial^2 R(\mathbf{x}^s,\mathbf{x})/\partial x_i'^2)^2}$. Because the determinant of a matrix is equal to the product of its eigenvalues, we see that $\det\mathbf{H}(\mathbf{x},q_{s1},q_{s2}) = 1$. Simultaneously, we see that $\operatorname{sgn}\mathbf{H}(\mathbf{x},q_{s1},q_{s2}) = 0$ because of the equal number of positive and negative eigenvalues. From equation C-2, it follows that $\varphi(\mathbf{x},q_{s1},q_{s2}) = 0$. Therefore the coefficients (formula C-5) are

$$\chi_{m1}(\mathbf{x}) \sim k_{m1}(q_s(\mathbf{x})) = k_{m1}\left(\frac{\sin\gamma(\mathbf{x})}{c_1}\right). \quad \text{(C-7)}$$

By analogy, we can prove that

$$\chi_{1m}(\mathbf{x}) \sim k_{1m}(q_s(\mathbf{x})) = k_{1m}\left(\frac{\sin\gamma(\mathbf{x})}{c_1}\right). \quad \text{(C-8)}$$

Note that, in the vicinity of the stationary point, the function C-2 has the representation

$$\varphi(\mathbf{x}',q_1,q_2) = \frac{1}{2}v^T\mathbf{H}(\mathbf{x},q_{s1},q_{s2})v, \quad \text{(C-9)}$$

where $v^T = (x_1' - x_1, x_2' - x_2, q_1 - q_{s1}, q_2 - q_{s2})$.

As shown by van Kampen (1949, 1950), the stationary phase approximation is valid only inside the region $\omega\varphi(\mathbf{x}',q_1,q_2) \le \pi$ in $S \times Q$. The condition is satisfied inside a 4D cylinder with a bounded base on the plane (x_1,x_2) and infinite generating lines with respect to (q_1,q_2). The radius of the base on $(\omega x_1, \omega x_2)$ can be defined from the condition

$$\frac{h(\mathbf{x})}{\omega c_1}\xi_F^2(\mathbf{x}) = \pi, \quad \text{(C-10)}$$

where $\xi_F(\mathbf{x}) = \omega r_F(\mathbf{x})$, and the quantity

$$h(\mathbf{x}) = \frac{1}{2}\left[\frac{\partial^2 R(\mathbf{x}^s,\mathbf{x})}{\partial x_1'^2} + \frac{\partial^2 R(\mathbf{x}^s,\mathbf{x})}{\partial x_2'^2}\right] \quad \text{(C-11)}$$

is the mean curvature of the wavefront with respect to the curved interface. From formulas C-10 and C-11, it follows that

$$\xi_F(\mathbf{x}) = \sqrt{\frac{\pi\omega c_1}{h(\mathbf{x})}}. \quad \text{(C-12)}$$

Following van Kampen (1958), this circle coincides with the Fresnel zone on the curved interface S. Because the Fresnel zone is not bounded on the plane (q_1,q_2), the formulas C-5 and C-8 represent nonuniform asymptotics of the effective coefficients, which do not account for the fact that the circle of critical points $q = 1/c_2$ falls inside the cylinder $\omega\varphi(\mathbf{x}',q_1,q_2) \le \pi$. Therefore we need to find a uniform asymptotic that would account for the critical phenomenon.

To find the uniform asymptotic, consider the convolution (formula 19). In the polar coordinates

$$x_1' = r\cos\varphi, \qquad x_2' = r\sin\varphi, \quad \text{(C-13)}$$

the effective coefficient (formula 19) can be represented as

$$\chi_{m1}(\mathbf{x}) = \int_0^\infty k_{m1}(\xi) I(\xi;\mathbf{x}) \xi d\xi, \quad \text{(C-14)}$$

$$I(\xi;\mathbf{x}) = \int_0^{2\pi} \bar{p}_0(\mathbf{x}';\mathbf{x})\frac{d\varphi}{2\pi}. \quad \text{(C-15)}$$

To obtain an analytical form of the integrand (equation C-15), represent the phase of the function $\bar{p}_0(\mathbf{x}';\mathbf{x})$ inside the Fresnel zone by its Taylor series of the second order, following van Kampen (1949, 1950):

$$\bar{p}_0(\mathbf{x}';\mathbf{x}) = e^{i\omega[q_s(\mathbf{x})\cos(\varphi-\psi)r+1/c_1(h(\mathbf{x})+\beta(\mathbf{x})\cos 2\varphi)r^2/2]}, \quad \text{(C-16)}$$

where the quantity $\beta(\mathbf{x}) = 1/2[\partial^2 R(\mathbf{x}^s,\mathbf{x})/\partial x_1'^2 - \partial^2 R(\mathbf{x}^s,\mathbf{x})/\partial x_2'^2]$ is the astigmatic coefficient of the wavefront with respect to the curved interface.

Substituting equation C-16 into the integral (equation C-15) and expanding the function $e^{i(\omega/c_1)\beta(\mathbf{x})\cos 2\varphi(r^2/2)}$ into power series, we can identically represent it in the form

$$I(\xi;\mathbf{x}) = e^{i\pi/2[\xi/\xi_F]^2}[J_0(\xi q_s(\mathbf{x})) + \varepsilon(\xi;\mathbf{x})], \quad \text{(C-17)}$$

where $J_0(\xi q_s(\mathbf{x})) = \int_0^{2\pi} e^{i\xi\cos(\varphi-\psi)}\partial\varphi/2\pi$ is the zero-order Bessel function. Analysis given by van Kampen (1949) shows that the angular integral $\varepsilon(\xi;\mathbf{x})$ depends on the astigmatic coefficient $\beta(\mathbf{x})$, and is of the order of $O(\omega^{-1})$, and, therefore, can be neglected. Substitution of equation C-17 into equation C-14 gives us the simplest admissible approximation for the effective coefficient

$$\chi_{m1}(\mathbf{x}) = \chi_{m1}(q_s(\mathbf{x}),\xi_F(\mathbf{x})) \cong \int_0^{\infty} k_{m1}(\xi)e^{i\pi/2[\xi/\xi_F(\mathbf{x})]^2}J_0(\xi q_s(\mathbf{x}))\xi d\xi. \quad \text{(C-18)}$$

It clearly follows from this representation that either for high frequencies, when $h(\mathbf{x}) \ll \omega$, or in the case when the front of the incident wave is plane with respect to the interface, meaning $h(\mathbf{x}) = 0$, the exponential term $e^{i\pi/2[\xi/\xi_F]^2}$ reaches the value of 1. Then the representation becomes the inverse Bessel transform of the one in equation 10, and we find that $\chi_{m1}(q_s(\mathbf{x}),\xi_F(\mathbf{x})) \simeq k_{m1}(q_s(\mathbf{x}))$. It was shown numerically that the function $k_{m1}(\xi)$ rapidly decreases for $\xi > \xi_F(\mathbf{x})$ so that the integral (equation C-18) over the infinite interval $(\xi_F(\mathbf{x}),\infty)$ can be neglected. It can also be noticed that the neglected integral with the astigmatic coefficient $\beta(\mathbf{x})$ gives a small low-frequency correction to the main contribution (equation C-18).

Because the integral (equation C-18) depends on the quantity $h(\mathbf{x})$, we need to evaluate it in explicit geometric terms:

$$R(\mathbf{x}^s,\mathbf{x}') = \sqrt{\bar{R}^2(\mathbf{x}^s,\mathbf{x}') - 2R(\mathbf{x}^s,\mathbf{x})\cos\gamma(\mathbf{x})z(\mathbf{x}') + z^2(\mathbf{x}')}, \quad \text{(C-19)}$$

where $\bar{R}(\mathbf{x}^s,\mathbf{x}')$ is the distance between the source and the projection of $\mathbf{x}'$ onto the plane tangent to the interface S at point $\mathbf{x}$; $z(\mathbf{x}')$ is introduced in Appendix B. Then in geometric terms, the quantity $h(\mathbf{x})$ is

$$h(\mathbf{x}) = \frac{1 - \frac{1}{2}\sin^2\gamma(\mathbf{x})}{R(\mathbf{x}^s,\mathbf{x})} - \cos\gamma(\mathbf{x})H_s(\mathbf{x}), \quad \text{(C-20)}$$

where $H_S(\mathbf{x}) = 1/2(\partial^2 z(\mathbf{x})/\partial x_1'^2 + \partial^2 z(\mathbf{x})/\partial x_2'^2)$ is the mean curvature of the interface S at the point $\mathbf{x}$. Note that the quantity $h(\mathbf{x})$ depends only on the incident angle $\gamma(\mathbf{x})$, the distance $R(\mathbf{x}^s,\mathbf{x})$, and the mean interface curvature $H_S(\mathbf{x})$.

Thus we have shown that the effective coefficients (equation C-18) essentially depend on the two parameters $q_s(\mathbf{x})$ and $\xi_F(\mathbf{x})$. This fact can be used for practical calculations. For example, instead of calculating the effective coefficients for the real curved interface, which implies convolution in the curvilinear Chebyshev coordinates, we can calculate the effective coefficients for any wavefield having such a trace at the interface that its parametric functions $q_s(\mathbf{x})$ and $\xi_F^*(\mathbf{x})$ are equal to the actual $q_s(\mathbf{x})$ and $\xi_F(\mathbf{x})$. For simplicity, we choose an apparent spherical wave $p_0^*(\mathbf{x}') = \rho_1 e^{ik_1 R^*(\mathbf{x}')}/4\pi R^*(\mathbf{x}')$ impinging on an apparent plane interface S^* and having incident angle $\gamma^*(\mathbf{x})$ and distance $R^*(\mathbf{x}^s,\mathbf{x})$. For this wave, $\xi_F^*(\mathbf{x})$ is calculated in accordance to formula C-20, with the only exception that $H_S^*(\mathbf{x}) = 0$. The desired equality $\xi_F^*(\mathbf{x}) = \xi_F(\mathbf{x})$ gives us the equation

$$\frac{1 - \frac{1}{2}\sin^2\gamma^*(\mathbf{x})}{R^*(\mathbf{x}^s,\mathbf{x})} = \frac{1 - \frac{1}{2}\sin^2\gamma(\mathbf{x})}{R(\mathbf{x}^s,\mathbf{x})} - \cos\gamma(\mathbf{x})H_s(\mathbf{x}). \quad \text{(C-21)}$$

Considering the natural equality $\gamma^*(\mathbf{x}) = \gamma(\mathbf{x})$ and solving equation C-21, we obtain

$$R^*(\mathbf{x}^s,\mathbf{x}) = R(\mathbf{x}^s,\mathbf{x}) \times \frac{\left[1 - \frac{1}{2}\sin^2\gamma(\mathbf{x})\right]}{\left[1 - \frac{1}{2}\sin^2\gamma(\mathbf{x})\right] - \cos\gamma(\mathbf{x})R(\mathbf{x}^s,\mathbf{x})H_S(\mathbf{x})}. \quad \text{(C-22)}$$

From equation C-22, it follows that the source of the apparent spherical wave lies on the same ray as the actual source, but at some apparent distance $R^*(\mathbf{x}^s,\mathbf{x})$. Note that if $R^*(\mathbf{x}^s,\mathbf{x}) > 0$, the apparent source lies on the same side of the interface as the actual source. In this case, the apparent spherical wave diverges toward the interface. If $R^*(\mathbf{x}^s,\mathbf{x}) < 0$, the apparent source seems to lie on the geometric continuation of the ray. In this case, the apparent spherical wave converges from the interface toward the source.

The effective coefficients at point $\mathbf{x}$ can be written as a function of the two main parameters of the incident wave

$$\chi_{m1}(\mathbf{x}) \cong \chi_{m1}(q_s(\mathbf{x}),\xi_F(\mathbf{x})) = \frac{\omega^2}{2\pi}\int\int_{S^*} k_{m1}(\xi)\bar{p}_0^*(\mathbf{x}';\mathbf{x})dx_1'dx_2',$$

$$\chi_{1m}(\mathbf{x}) \cong \chi_{1m}(q_s(\mathbf{x}),\xi_F(\mathbf{x})) = \frac{\omega^2}{2\pi}\int\int_{S^*} k_{1m}(\xi)\bar{a}_0^*(\mathbf{x}';\mathbf{x})dx_1'dx_2', \quad \text{(C-23)}$$

where

$$\bar{p}_1^*(\mathbf{x}';\mathbf{x}) = \frac{p_0^*(\mathbf{x}')}{p_0^*(\mathbf{x})},$$
$$\bar{a}_1^*(\mathbf{x}';\mathbf{x}) = \frac{a_0^*(\mathbf{x}')}{a_0^*(\mathbf{x})}, \qquad \text{(C-24)}$$

and $\mathbf{x}'$ belongs to the apparent plane S^*.

We will now concentrate on properties of the effective coefficients. Here we would like to show that in some cases their approximate description (equation C-23) can be justified by comparison with exact results.

As the first example, consider the case of a plane interface S, so that $H_s(\mathbf{x}) \equiv 0$. It is evident that the apparent plane S^* coincides with the actual interface S. Therefore $R^*(\mathbf{x}^s,\mathbf{x}) = R(\mathbf{x}^s,\mathbf{x})$, and the apparent spherical wave trivially coincides with the actual spherical wave. In this particular case, the approximate relations (equation C-23) become exact as in formula 19. Note that the problem of numerical realization of the convolutions remains to be solved.

As the second example, consider such an incident wave that the effective coefficients (formula 19) can be calculated analytically to compare the analytical result with the approximations (equation C-23). To show this, we chose the incident wave to impinge on the interface with the constant incident angle γ^0. Then

$$\bar{p}_0(\mathbf{x}';\mathbf{x}) = e^{i\omega[q_1^0(x_1'-x_1)+q_2^0(x_2'-x_2)]}, \qquad \text{(C-25)}$$

where (q_1^0, q_2^0) are the tangent components of the slowness vector, such that $q^0 = \sin\gamma^0/c_1$. Substitution of equation C-25 into the exact representation (equation C-1) gives

$$\chi_{m1}(\mathbf{x}) = \frac{\omega^2}{2\pi}\int\int_Q k_{m1}(q)dq_1dq_2\frac{1}{2\pi}\int\int_S \times e^{i\omega[(x_1-x_1')(q_1-q_1^0)+(x_2-x_2')(q_2-q_2^0)]}dx_1'dx_2'. \qquad \text{(C-26)}$$

Using the identity from spectral analysis (see e.g., Felsen and Marcuvitz, 1973),

$$\delta(q_1-q_1^0,q_2-q_2^0) = \frac{\omega^2}{2\pi}\int\int_S e^{i\omega[(x_1-x_1')(q_1-q_1^0)+(x_2-x_2')(q_2-q_2^0)]} \times dx_1'dx_2', \qquad \text{(C-27)}$$

we obtain the exact values of the effective coefficients

$$\chi_{m1}(\mathbf{x}) = k_{m1}(q^0) = k_{m1}\left(\frac{\sin\gamma^0}{c_1}\right). \qquad \text{(C-28)}$$

If the interface is plane, equation C-25 represents a plane wave, and the effective coefficients exactly coincide with the plane-wave coefficients. In particular, this means that the asymptotic (equation C-7) becomes exact.

REFERENCES

Aizenberg, A. M., 1982, Scattering of seismic waves by broken edge of a flat boundary: Soviet Geology and Geophysics, **23**, 74–82.

———, 1993a, Special function of eddy diffusion equation in 3D inhomogeneous space: Russian Geology and Geophysics, **34**, 107–114.

———, 1993b, A system of irregular fundamental solutions to wave equation in a 3-D inhomogeneous medium: Russian Geology and Geophysics, **34**, 119–127.

Aizenberg, A. M., and M. A. Ayzenberg, 2002, Simulation of interference wave field trace reflected/transmitted by plane interface of two acoustic media: Dynamics of solid media: Proceedings of Russian Academy of Sciences, **121**, 50–55.

Aizenberg, A., M. Ayzenberg, H. Helle, K. Klem-Musatov, and J. Pajchel, 2002, Single reflection at curvilinear interface. Tip wave superposition method with effective reflection coefficient: Norsk Hydro AS Open Report.

———, 2004, Modeling of single reflection by tip wave superposition method using effective coefficient: 66th Annual Conference and Exhibition, EAGE, Extended Abstracts.

Aizenberg, A. M., M. A. Ayzenberg, H. B. Helle, K. D. Klem-Musatov, J. Pajchel, and B. Ursin, 2006a, 3-D seismic diffraction modeling in multilayered media in terms of surface integrals: 68th Annual Conference and Exhibition, EAGE, Extended Abstracts.

Aizenberg, A., M. Ayzenberg, H. Helle, and J. Pajchel, 2005, Reflection and transmission of acoustic wavefields at a curved interface of two inhomogeneous media: Continuum Dynamics, Acoustics of Inhomogeneous Media, **123**, 73–79.

Aizenberg, A., H. Helle, K. Klem-Musatov, and J. Pajchel, 1996, The tip wave superposition method based on the refraction transform: 58th Annual Conference and Exhibition EAGE, Extended Abstracts, Session C001.

Aizenberg, A., K. Klem-Musatov, M. Ayzenberg, H. Helle, and J. Pajchel, 2006b, Integral reflection-transmission operators instead of reflection-transmission coefficient — A possibility to increase the resolution of seismic exploration: Russian Geology and Geophysics, **47**, 537–546.

Aki, K., and P. Richards, 2002, Quantitative seismology, 2nd ed. University Science Books.

Berkhout, A. J., 1987, Applied seismic wave theory: Elsevier Science Publishing Co.

Bleistein, N., and R. A. Handelsman, 1975, Asymptotic expansions of integrals: Dover Publications.

Červený, V., 2001, Seismic ray theory: Cambridge University Press.

Costabel, M., and E. P. Stephan, 1990, Integral equations for transmission problems in linear elasticity: Journal of Integral Equations and Applications, **2**, 211–223.

do Carmo, M. P., 1976, Differential geometry of curves and surfaces: Prentice-Hall Inc.

Felsen, L. B., and N. Marcuvitz, 1973, Radiation and scattering of waves: Prentice-Hall Inc.

Frazer, L. N., and M. K. Sen, 1985, Kirchhoff-Helmholtz reflection seismograms in a laterally inhomogeneous multi-layered elastic medium — I. Theory: Geophysical Journal of the Royal Astronomical Society, **80**, 121–147.

Kampfmann, W., 1988, A study of diffraction-like events on DECORP 2-S by Kirchhoff theory: Journal of Geophysics, **62**, 163–174.

Kleinman, R. E., and P. A. Martin, 1988, On single integral equations for the transmission problem of acoustics: Journal of Applied Mathematics, **48**, 307–325.

Klem-Musatov, K. D., 1994, Theory of seismic diffractions: Open File Publications No. 1: SEG.

Klem-Musatov, K. D., and A. M. Aizenberg, 1985, Seismic modelling by methods of the theory of edge waves: Journal of Geophysics, **57**, 90–105.

Klem-Musatov, K. D., A. M. Aizenberg, H. B. Helle, and J. Pajchel, 1993, Seismic simulation by the tip wave superposition method in complex 3D geological models: 55th Annual Conference and Exhibition, EAGE, Extended Abstracts, Session P103.

Klem-Musatov, K. D., A. M. Aizenberg, J. Pajchel, and H. B. Helle, 1994, Edge and tip diffractions — Theory and applications in seismic prospecting: Norsk Hydro.

Klem-Musatov, K. D., A. M. Aizenberg, H. B. Helle, and J. Pajchel, 2004, Reflection and transmission at curvilinear interface in terms of surface integrals: Wave Motion, **39**, 77–92.

———, 2005, Reflection and transmission in multilayered media in terms of surface integrals: Wave Motion, **41**, 293–305.

Schleicher, J., M. Tygel, B. Ursin, and N. Bleistein, 2001, The Kirchhoff-Helmholtz integral for anisotropic elastic media: Wave Motion, **34**, 353–364.

Sen, M. K., and L. N. Frazer, 1991, Multifold phase space path integral synthetic seismograms: Geophysical Journal International, **104**, 479–487.

Ursin, B., 2004, Tutorial: Parameter inversion and angle migration in aniso-

tropic elastic media: Geophysics, **69**, 1125–1142.
Ursin, B., and M. Tygel, 1997, Reciprocal volume and surface scattering integrals for anisotropic elastic media: Wave Motion, **26**, 31–42.
van Kampen, N. G., 1949, An asymptotic treatment of diffraction problem — I: Physica, **14**, 575–589.
——–, 1950, An asymptotic treatment of diffraction problems — II: Physica, **16**, 817–821.
——–, 1958, The method of stationary phase and the method of Fresnel zones: Physica, **24**, 437–444.
Weatherborn, C. E., 1930, Differential geometry of three dimensions, vol. II: Cambridge University Press.
Wenzel, F., K.-J. Stenzel, and U. Zimmermann, 1990, Wave propagation in laterally heterogeneous layered media: Geophysical Journal International, **103**, 675–684.